Synergy of Stochastic and Systematic Energization of Plasmas during Turbulent Reconnection

Theophilos Pisokas, Loukas Vlahos [ID], and Heinz Isliker [ID]
Department of Physics, Aristotle University of Thessaloniki, GR-52124 Thessaloniki, Greece

Abstract

The important characteristic of turbulent reconnection is that it combines large-scale magnetic disturbances ($\delta B/B \sim 1$) with randomly distributed unstable current sheets (UCSs). Many well-known nonlinear MHD structures (strong turbulence, current sheet(s), shock(s)) lead asymptotically to the state of turbulent reconnection. We analyze in this article, for the first time, the energization of electrons and ions in a large-scale environment that combines large-amplitude disturbances propagating with sub-Alfvénic speed with UCSs. The magnetic disturbances interact stochastically (second-order Fermi) with the charged particles and play a crucial role in the heating of the particles, while the UCSs interact systematically (first-order Fermi) and play a crucial role in the formation of the high-energy tail. The synergy of stochastic and systematic acceleration provided by the mixture of magnetic disturbances and UCSs influences the energetics of the thermal and nonthermal particles, the power-law index, and the length of time the particles remain inside the energy release volume. We show that this synergy can explain the observed very fast and impulsive particle acceleration and the slightly delayed formation of a superhot particle population.

Key words: acceleration of particles – magnetic reconnection – methods: numerical – Sun: flares – turbulence

1. Introduction

Turbulent reconnection can be generated by different, well-known, nonlinear MHD processes and structures, which serve as their driver, e.g., the evolution of a spectrum of large-amplitude MHD waves, the fragmentation of a current sheet(s), or shock(s) (see the reviews of Matthaeus & Velli [2011], Cargill et al. [2012], Hoshino & Lyubarsky [2012], Lazarian et al. [2012, 2015], and Karimabadi et al. [2013a, 2013b] and the recent articles by Zank et al. [2015] and Matsumoto et al. [2015] on turbulent reconnection driven by shocks, for a brief, yet incomplete, outline of the relevant literature).

The term "turbulent reconnection" appeared first in Matthaeus & Lamkin (1986), and several years later the analytical theory of turbulent reconnection was formulated by Lazarian & Vishniac (1999). In both articles, the role of weak turbulence in the evolution of a reconnecting current sheet was analyzed. In the present article, we expand the term "turbulent reconnection" to denote the coexistence of "large-scale coherent magnetic disturbances" (Kuramitsu & Hada 2000; Greco et al. 2010; Malapaka & Müller 2013) with "unstable current sheets" (UCSs). It has been shown that these two types of nonlinear structures drive and re-enforce each other (Karimabadi et al. 2013b).

There are at least three avenues that lead to the generation of turbulent reconnection. The first is strong turbulence (Biskamp & Welter 1989; Dmitruk et al. 2003, 2004; Arzner et al. 2006; Isliker et al. 2017b). The second is the fragmentation of UCSs: numerous studies have explored the evolution of one or multiple UCSs and have shown that they evolve into a turbulent reconnection environment (Matthaeus & Lamkin 1986; Lazarian & Vishniac 1999; Onofri et al. 2004; Cassak & Drake 2009; Loureiro et al. 2009; Kowal et al. 2011; Hoshino 2012). The third avenue lies downstream of a shock where turbulent reconnection can be driven when the shock is formed in the presence of upstream turbulent flows, e.g., as is the case with Earth's bow shock and the solar wind, or with coronal mass ejections traveling inside the turbulent solar wind (Matsumoto et al. 2015; Zank et al. 2015; Burgess et al. 2016).

Several authors explored the formation of turbulent reconnection in the solar atmosphere, driven by the turbulent convection zone (Parker 1983, 1988; Einaudi & Velli 1994; Galsgaard & Nordlund 1996, 1997a, 1997b; Georgoulis et al. 1998; Rappazzo et al. 2010, 2013). All these studies focused on the formation of UCSs; large-amplitude magnetic disturbances were also present yet never analyzed in detail until recently (Kontar et al. 2017).

The solar wind is probably the most striking example of a turbulently reconnecting plasma flow, and the coexistence of large-amplitude magnetic disturbances and UCSs has been analyzed in detail by several authors (Greco et al. 2010; Osman et al. 2014; Chasapis et al. 2015).

It is natural to expect that in relativistic jets and other astrophysical flows (e.g., accretion disks) turbulent reconnection will be present, but details have not been worked out yet (Giannios 2010; Sironi et al. 2015; Brunetti & Lazarian 2016). The acceleration mechanism preferred by most researchers as the best candidate for explaining the explosive phenomena in astrophysics remains diffusive shock acceleration, which can be the host of turbulent reconnection (Matsumoto et al. 2015; Zank et al. 2015). The relative importance of the two systematic accelerators (shock acceleration and turbulent reconnection) has not yet been established.

Karimabadi et al. (2013b) pointed out that intermittent plasma turbulence will in general consist of both coherent structures (UCSs) and large-amplitude waves (see also Wang et al. 2015; Liang et al. 2016; see also the picture given in Kowal et al. [2017] for the MHD evolution of a single small-scale UCS). With their simulations they have presented evidence for the excitation of eddies and waves by the motion of fragmented UCSs. They also noted that this complex environment, which we call here turbulent reconnection, heats the plasma very efficiently.

The evolution of an ensemble of charged particles in turbulent reconnection was investigated by several authors using test particle simulations in snapshots of MHD codes (Ambrosiano et al. 1988; Dmitruk et al. 2004; Turkmani et al. 2005; Arzner et al. 2006; Onofri et al. 2006; Isliker et al. 2017b).

Several authors (Vlahos et al. 2016; Isliker et al. 2017a; Pisokas et al. 2017) analyzed the statistical properties of ions and electrons scattered either off large-amplitude magnetic disturbances propagating with the Alfvén speed (Alfvénic scatterers [ASs]) or off UCSs, randomly distributed inside the energy release volume. The interaction of electrons and ions with the accelerators is either stochastic, when they interact with Alfvénic disturbances, as in the model proposed initially by Fermi (1949), or systematic, when they interact with UCSs (Fermi 1954). The stochastic energization of ions and electrons leads the initial Maxwellian energy distribution to an asymptotic state, and the final distribution is a mixture of a hot and an accelerated plasma, with a power-law tail with index ∼2. The acceleration time for parameters related with the solar corona is close to a few seconds (see details in Vlahos et al. 2016; Pisokas et al. 2017). In the case of systematic acceleration, when the energy release volume is dominated by UCSs, the particles are mostly accelerated, forming a power-law tail with index $\geqslant 1$ on subsecond timescales, and heating is practically absent (see Vlahos et al. 2016; Isliker et al. 2017a).

In most laboratory and astrophysical plasmas the explosive energy release is associated with intense and efficient heating of the bulk of the plasma and with the formation of a power-law tail on very fast timescales (see, e.g., the evolution of the photon distribution for solar flares analyzed by Lin et al. 2003). Lin et al. (2003) pointed out that in the initial rise of a flare substantial particle acceleration is taking place and in the subsequent impulsive phase a coronal superhot component appears. A possible explanation for the prompt acceleration and the delayed appearance of the superhot plasma may be related to the differences in the acceleration times between UCSs and the ASs, as reported above. In summary, the synergy of large-scale magnetic disturbances and UCSs in turbulent reconnection can provide the explanation for the appearance of impulsive heating of the superhot sources and of the nonthermal tails.

In this article, we assume that the energy release volume is in the state of turbulent reconnection and the nonlinear structures (magnetic disturbances and UCSs, interchangeably called here "active grid points" or "scatterers") are randomly distributed. The charged particles scatter off the active grid points and gain or lose energy. The scatterers are divided into two classes: a fraction P ($0 \leqslant P \leqslant 1$) are magnetic disturbances (ASs), and the rest ($1 - P$) are UCSs. When $P = 0$, all scatterers are UCSs, and when $P = 1$, all scatterers are magnetic disturbances (see Vlahos et al. 2016; Isliker et al. 2017a; Pisokas et al. 2017, for studies of the extreme cases).

2. Mixing Stochastic and Systematic Scatterers

2.1. The Initial Setup

The scatterers are randomly chosen and uniformly distributed grid points of a 3D lattice that has linear size L and consists of ($N \times N \times N$) nodes, with grid size $\ell = L/(N - 1)$. The N_{sc} scatterers form a small fraction $R = N_{sc}/N^3$ of the total number of nodes, and they are either ASs or UCSs, as

described above. The mean free path between scatterers can be determined as $\lambda_{sc} = \ell/R$. An ensemble of particles (electrons or ions) are injected into the simulation volume at random grid points, with random direction of motion, and they are allowed to move along the straight lattice edges until they encounter an active grid point. Encounters with scatterers cause a particle to change its direction of motion and to renew its energy by the amount ΔW, which depends on the physical characteristic of the scatterer. This process repeats up to the final time or until a particle reaches the lattice boundary and escapes (see Vlahos et al. 2016; Isliker et al. 2017a; Pisokas et al. 2017, for a more complete description of the model).

We assume that the simulation volume has length $L = 10{,}000\,\text{km}$, the active grid point ratio is $R = 5\%{-}15\%$, and the injected particles follow a Maxwellian distribution with temperature $T \approx 1 \times 10^6$ K. If a scatterer is an AS, the change in energy of a particle amounts to

$$\frac{\Delta W^{(\text{AS})}}{W} \approx \frac{2}{c^2}(V^2 - \boldsymbol{V} \cdot \boldsymbol{u}), \tag{1}$$

where for head-on collisions $\boldsymbol{V} \cdot \boldsymbol{u} < 0$ and the particle gains energy, and for overtaking collisions $\boldsymbol{V} \cdot \boldsymbol{u} > 0$ and the particle loses energy (Pisokas et al. 2017). The ASs, as stochastic scatterers, transfer energy either to or from an interacting particle, but the overall result for the particles is a gain in energy, with a typical increment of the order of $(\Delta W/W) \approx (V_A/c)^2 \sim 5 \times 10^{-4}$.

With a UCS as the scatterer, the energy gain is caused by the electric field (Kowal et al. 2011; Isliker et al. 2017a), and it is given by

$$\Delta W^{(\text{EF})} = |q| E_{\text{eff}}\, \ell_{\text{eff}}, \tag{2}$$

where $E_{\text{eff}} \approx (V/c)\,\delta B$ is a measure of the effective electric field of the UCS, and δB is the fluctuating magnetic field, which is of stochastic nature, as related to the stochastic fluctuations induced by reconnection. The energy increments in Equation (2) are always positive, as it was shown to hold in different particle-in-cell simulations (Dahlin et al. 2015; Guo et al. 2015; Matsumoto et al. 2015), and they do not depend on the instantaneous energy of a particle; instead, they are proportional to the magnetic field fluctuations δB. The latter are assumed to follow a Kolmogorov spectrum, i.e., they obey a power-law distribution with index $5/3$ in the range $[10^{-5}\,\text{G}, 100\,\text{G}]$. The effective length ℓ_{eff} of the interaction of a particle with a UCS is assumed to be an increasing linear function of E_{eff} (so that small E_{eff} are associated with small-scale UCSs), restricted to values between 10 m and 1 km (see more details in Isliker et al. 2017a).

2.2. Mixing ASs with UCSs Dominated by Electric Fields

In Figure 1 the energy evolution of some typical particles traveling inside a mixture of stochastic and systematic scatterers ($P = 0.5$) is shown. The synergy of stochastic acceleration by the ASs (classical random-walk-like behavior) with systematic acceleration at the UCSs (sudden increases of energy) is apparent.

As described above, the particles travel and interact with scatterers until they exit the acceleration volume at some time, which is different for each particle. The median value of these times is the characteristic escape time (t_{esc}) for the ensemble,
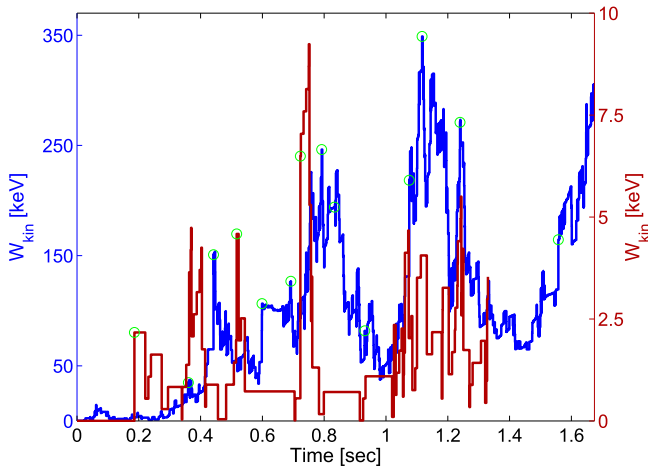
Figure 1. Kinetic energy of typical electrons as a function of time.

and it coincides with the half time $t_{1/2}$ of the system, defined as the time when half of the initial electron population has escaped. The energy distribution for the electrons that remain inside the volume exhibits a clear and extended power-law tail for $P = 0$, with negligible heating at the low energies, but as P grows, the electrons are also heated under the influence of the magnetic disturbances, until they reach a combination of a hot plasma with a relatively small number of particles in the power-law tail for $P = 0.5$, as shown in Figure 2(a).

The temperature of the heated low-energy part of the distribution grows linearly with increasing P, starting from a value close to the initial temperature for $P = 0$ and reaching a much higher temperature of ≈ 130 keV for $P = 1$ (see Figure 2(b)). On the other hand, the mean energy of the particles in the high-energy tail increases with increasing P until it reaches a maximum value of ≈ 17–18 MeV, forming a plateau for the middle range of P values (0.3–0.7). For higher P values, the mean energy of the tail drops to ≈ 2 MeV. The synergy of the two classes of scatterers varies the behavior of the system from an efficient accelerator, when the UCSs dominate, to an efficient and excessive heating mechanism combined with acceleration, when both types of scatterers are involved. The power-law tail consists of a small percentage ($\sim 2\%$–5%) of the total number of particles injected initially for almost all P values, with the exception of the pure UCS case, $P = 0$ (Isliker et al. 2017a), where the high-energy particles are almost 15% of the total number of particles at $t = t_{\rm esc}$.

For any combination of the two types of scatterers, the distribution of the high-energy particles develops a power-law shape, which ultimately attains an asymptotic index $k_{\rm asym}$. The time in which this occurs is a measure for the acceleration time of the system, $t_{\rm acc}$. According to Figure 2(b), when the fraction of the ASs is low ($P < 0.2$), the index $k_{\rm asym}$ is 1.7, as in a pure UCS system, but as the influence of the ASs becomes stronger, we find $k_{\rm asym} \approx 2.1$. The fraction of ASs also affects the acceleration time, which varies around 1.5–2 s for $P \geqslant 0.2$, but it is much shorter for lower P values, e.g., ≈ 0.5 s for $P = 0.1$ and a few milliseconds for $P = 0$. Electrons leave the system earlier when ASs are present. We can conclude from this parametric study of the energy distribution that the power-law tail is a result of the synergy between the ASs and the UCSs, while the heating of the particles is a sole effect of the ASs.
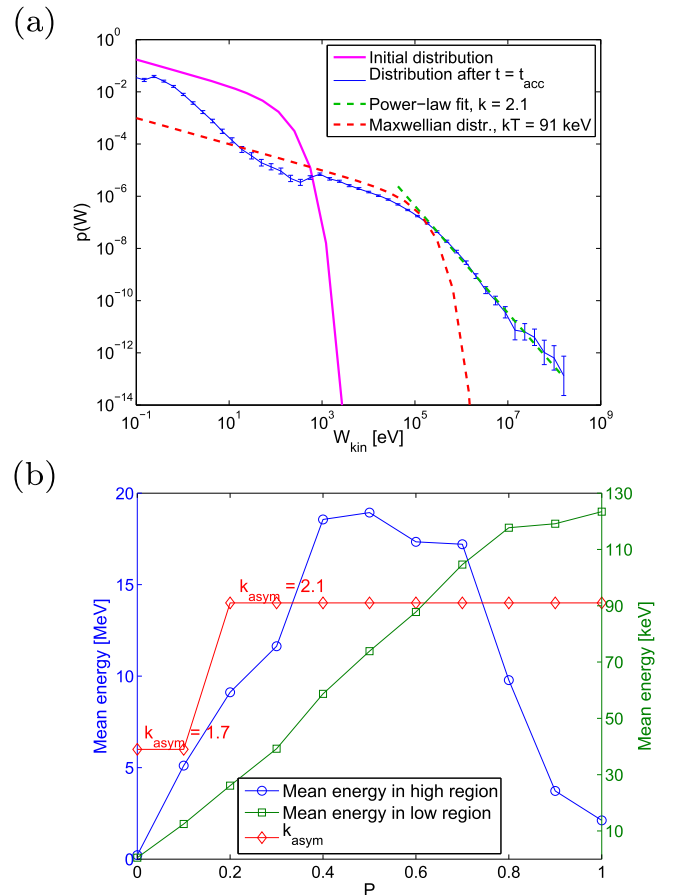

Figure 2. (a) Energy distribution of the electrons that stay inside until $t = t_{\rm acc} \approx 1.7$ s (blue), for $P = 0.5$, initial distribution (magenta), Maxwellian fit to the heated low-energy region (red dashed), and fit to the power-law tail (green dashed). (b) Mean energy at $t = t_{\rm esc}$ for the high-energy tail (blue) and the heated low-energy region (green) for different ratios P of the two kinds of scatterers; the red points denote the asymptotic value $k_{\rm asym}$ of the power-law index.

2.3. The Evolution of the Escape Time

As mentioned before, each particle exits the acceleration volume at a different time with a different energy. The escape time distribution adopts a power-law shaped tail, as shown in Figure 3(a).

The distribution of the escape energy, i.e., the energy with which any particle escapes from the acceleration volume, exhibits the same behavior as the one of the particles that stay inside. The escape time and the escape energy depend on each other; the escape time as a function of the escape energy (determined through binned statistics) is shown in Figure 3(b) for $P = 0.5$, compared also to the two "pure" cases ($P = 0$ and 1). We observe two distinct regions: for nonrelativistic energies, 10–10^5 eV, a power-law scaling is assumed, $t_{\rm esc} \propto W_{\rm esc}^{0.4}$.

As for the relativistic energies, 10^5–10^9 eV, the functional form depends on P, e.g., for $P = 0.5$ there is a power-law scaling with index 0.2. In any case, the escape energy of the electrons is strongly related to the length of time the particles spend in the system, which is also illustrated when considering the number of scatterings the escaping particles suffer before they escape from the simulation box as a function of their escape energy (see Figure 3(c); determined again through binned statistics), and the escape energy increases with increasing number of scatterings, with a saturation at the highest energies.

(a)
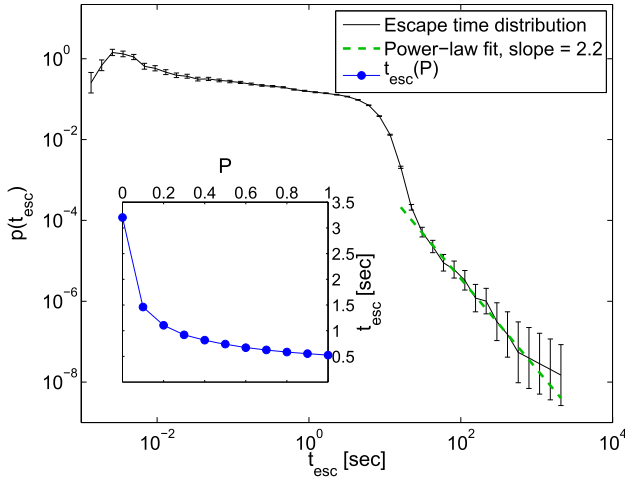
(b)
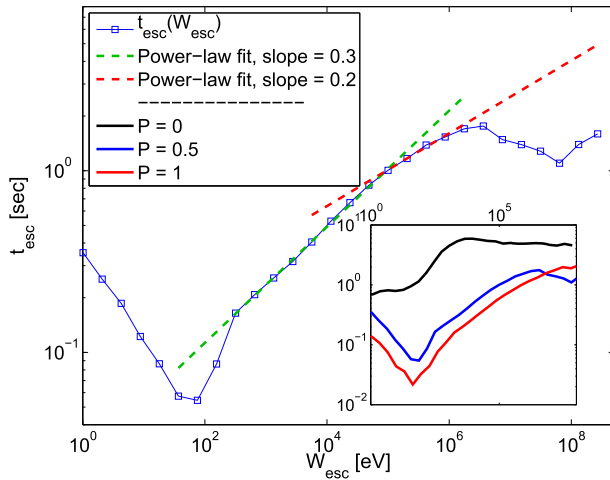
(c)
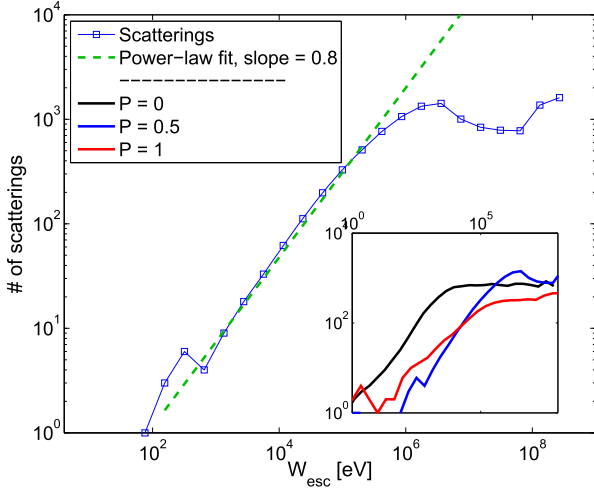
Figure 3. (a) Escape time distribution for $P = 0.5$; inset: escape time distribution for different values of P. (b) Escape time as a function of the escape energy of the electrons for $P = 0.5$; inset: comparison between $P = 0$ (black), 0.5 (blue), and 1 (red). (c) Number of scatterings as a function of the escape energy of the electrons for $P = 0.5$; inset: comparison between $P = 0$ (black), 0.5 (blue), and 1 (red).

All of the above results refer to electron populations. When ions are considered, no significant changes are observed. The energy distribution follows the same trends as in the electron case, with corresponding characteristics for the same values of P, similarly changing as P varies. Only the timescale is different, e.g., the escape time now extends from ≈ 130 s for $P = 0$ to ≈ 5 s for $P = 0.5$, and it reaches ≈ 3 s for $P = 1$. UCSs not only are efficient accelerators but also keep the high-energy plasma longer inside the simulation box.

3. Discussion and Summary

In most explosive laboratory and astrophysical systems plasma heating is strongly correlated with particle acceleration. In the current literature the problems of heating and particle acceleration are studied separately. In explosive phenomena, particle acceleration has been related to reconnection, shocks, or weak turbulence, but no mechanism for the impulsive heating has been proposed so far (Lin et al. 2003).

In this article, we have shown that turbulent reconnection can be the solution to the combined problem, since the synergy of ASs and UCSs can provide both the intense heating and the acceleration of the tail. The mixing of stochastic and systematic acceleration provides an asymptotic energy distribution that is heated substantially and exhibits a power-law tail with index ~ 2, which is close to the one estimated from the observations. The escape time of the particles depends on the fraction of the two types of scatterers and the energy of the particles. The lower the fraction of ASs, the larger the escape time of the particles. The most energetic particles stay longest inside the acceleration volume (Krucker & Lin 2008). In the analysis presented in this article, we follow the evolution of the energy distribution for several seconds in a large-scale open system, where the magnetic disturbances and the UCSs have time to bring the energy distribution into an asymptotic state.

The scenario proposed here for most explosive phenomena in the solar atmosphere starts with the formation of large-scale current sheets, which fragment very quickly, leading to turbulent reconnection. The UCSs impulsively (in a few milliseconds) accelerate the tail of the energy distribution, and soon after (a few seconds later) the ASs start participating by forming the superhot sources and reinforcing the tail of the energy distribution (see a clear outline of the observations related to this scenario in Lin et al. 2003). The majority of the MHD simulations of explosive phenomena in the solar atmosphere rarely follow the fragmentation of the large-scale current sheet, which is usually formed, nor do they consider the generation of magnetic disturbances, due to the limitations in the spatial resolution of these codes. Therefore, the formation of turbulent reconnection and its role in coronal heating and particle acceleration, as analyzed here, have so far been ignored.

The spatial transport inside a turbulent plasma will also influence the distribution of the accelerated particles (Bian et al. 2017), and the coupling of energy and spatial transport in turbulent reconnecting plasmas remains an open problem. The prompt acceleration and the impulsive heating by turbulent reconnection inside a large-scale flaring magnetic topology and the anomalous transport in space will place the simple deterministic scenario for the interpretation of the hard X-rays during solar flares, as proposed by Brown (1971) almost 45 yr ago and named the "thick target model," in a new frame of analysis. We claim that turbulent reconnection will provide answers to many open questions, possibly caused by the simplicity of the physical process adopted in the thick target model.

ORCID iDs

Loukas Vlahos ⓘ https://orcid.org/0000-0002-8700-4172
Heinz Isliker ⓘ https://orcid.org/0000-0001-9782-2294

References

Ambrosiano, J., Matthaeus, W. H., Goldstein, M. L., & Plante, D. 1988, JGRA, 93, 14383
Arzner, K., Knaepen, B., Carati, D., Denewet, N., & Vlahos, L. 2006, ApJ, 637, 322
Bian, N. H., Emslie, A. G., & Kontar, E. P. 2017, ApJ, 835, 262
Biskamp, D., & Welter, H. 1989, PhFlB, 1, 1964
Brown, J. C. 1971, SoPh, 18, 489
Brunetti, G., & Lazarian, A. 2016, MNRAS, 458, 2584
Burgess, D., Gingell, P. W., & Matteini, L. 2016, ApJ, 822, 38
Cargill, P., Vlahos, L., Baumann, G., Drake, J., & Nordlund, Å. 2012, SSRv, 173, 223
Cassak, P. A., & Drake, J. F. 2009, ApJL, 707, L158
Chasapis, A., Retinò, A., Sahraoui, F., et al. 2015, ApJL, 804, L1
Dahlin, J. T., Drake, J. F., & Swisdak, M. 2015, PhPl, 22, 100704
Dmitruk, P., Matthaeus, W., Seenu, N., & Brown, M. R. 2003, ApJL, 597, L81
Dmitruk, P., Matthaeus, W. H., & Seenu, N. 2004, ApJ, 617, 667
Einaudi, G., & Velli, M. 1994, SSRv, 68, 97
Fermi, E. 1949, PhRv, 75, 1169
Fermi, E. 1954, ApJ, 119, 1
Galsgaard, K., & Nordlund, Å. 1996, JGR, 101, 13445
Galsgaard, K., & Nordlund, Å. 1997a, JGR., 102, 219
Galsgaard, K., & Nordlund, Å. 1997b, JGR., 102, 231
Georgoulis, M. K., Velli, M., & Einaudi, G. 1998, ApJ, 497, 957
Giannios, D. 2010, MNRAS, 408, L46
Greco, A., Perri, S., & Zimbardo, G. 2010, JGRA, 115, A02203
Guo, F., Liu, Y.-H., Daughton, W., & Li, H. 2015, ApJ, 806, 167
Hoshino, M. 2012, PhRvL, 108, 135003
Hoshino, M., & Lyubarsky, Y. 2012, SSRv, 173, 521
Isliker, H., Pisokas, T., Vlahos, L., & Anastasiadis, A. 2017a, ApJ, 849, 35
Isliker, H., Vlahos, L., & Constantinescu, D. 2017b, PhRvL, 119, 045101
Karimabadi, H., Roytershteyn, V., Daughton, W., & Liu, Y.-H. 2013a, SSRv, 178, 307
Karimabadi, H., Roytershteyn, V., Wan, M., et al. 2013b, PhPl, 20, 012303
Kontar, E. P., Perez, J. E., Harra, L. K., et al. 2017, PhRvL, 118, 155101
Kowal, G., de Gouveia Dal Pino, E. M., & Lazarian, A. 2011, ApJ, 735, 102
Kowal, G., Falceta-Gonçalves, D. A., Lazarian, A., & Vishniac, E. T. 2017, ApJ, 838, 91
Krucker, S., & Lin, R. P. 2008, ApJ, 673, 1181
Kuramitsu, Y., & Hada, T. 2000, GeoRL, 27, 629
Lazarian, A., Eyink, G., Vishniac, E., & Kowal, G. 2015, RSPTA, 373, 20140144
Lazarian, A., & Vishniac, E. T. 1999, ApJ, 517, 700
Lazarian, A., Vlahos, L., Kowal, G., et al. 2012, SSRv, 173, 557
Liang, J., Lin, Y., Johnson, J. R., Wang, X., & Wang, Z.-X. 2016, JGRA, 121, 6526
Lin, R. P., Krucker, S., Hurford, G. J., et al. 2003, ApJL, 595, L69
Loureiro, N. F., Uzdensky, D. A., Schekochihin, A. A., Cowley, S. C., & Yousef, T. A. 2009, MNRAS, 399, L146
Malapaka, S. K., & Müller, W.-C. 2013, ApJ, 778, 21
Matsumoto, Y., Amano, T., Kato, T. N., & Hoshino, M. 2015, Sci, 347, 974
Matthaeus, W. H., & Lamkin, S. L. 1986, PhFl, 29, 2513
Matthaeus, W. H., & Velli, M. 2011, SSRv, 160, 145
Onofri, M., Isliker, H., & Vlahos, L. 2006, PhRvL, 96, 151102
Onofri, M., Primavera, L., Malara, F., & Veltri, P. 2004, PhPl, 11, 4837
Osman, K. T., Matthaeus, W. H., Gosling, J. T., et al. 2014, PhRvL, 112, 215002
Parker, E. N. 1983, ApJ, 264, 635
Parker, E. N. 1988, ApJ, 330, 474
Pisokas, T., Vlahos, L., Isliker, H., Tsiolis, V., & Anastasiadis, A. 2017, ApJ, 835, 214
Rappazzo, A. F., Velli, M., & Einaudi, G. 2010, ApJ, 722, 65
Rappazzo, A. F., Velli, M., & Einaudi, G. 2013, ApJ, 771, 76
Sironi, L., Petropoulou, M., & Giannios, D. 2015, MNRAS, 450, 183
Turkmani, R., Vlahos, L., Galsgaard, K., Cargill, P., & Isliker, H. 2005, ApJL, 620, L59
Vlahos, L., Pisokas, T., Isliker, H., Tsiolis, V., & Anastasiadis, A. 2016, ApJL, 827, L3
Wang, L. C., Li, L. J., Ma, Z. W., Zhang, X., & Lee, L. C. 2015, PhLA, 379, 2068
Zank, G. P., Hunana, P., Mostafavi, P., et al. 2015, ApJ, 814, 137